CMS Physics Analysis Summary

Contact: cms-pag-conveners-heavyions@cern.ch 2016/05/24

Measurement of the charged particle nuclear modification factor in PbPb collisions at $\sqrt{s_{\mathrm{NN}}} = 5.02$ TeV

The CMS Collaboration

Abstract

The nuclear modification factor, R_{AA}, of charged particles produced in the $|\eta| < 1$ pseudorapidity region is measured at $\sqrt{s_{\mathrm{NN}}} = 5.02$ TeV using 404 $\mu\mathrm{b}^{-1}$ of PbPb and 25.8 pb^{-1} of pp data collected by the CMS experiment at the end of 2015. The R_{AA} is presented in several bins of collision centrality, over the transverse momentum range of $0.7 - 400$ GeV. The measured R_{AA} in the $0 - 5\%$ most central collision class shows a maximum suppression by a factor of approximately 7.5 in the $6 - 9$ GeV p_{T} region, followed by a rising trend up to the highest transverse momenta measured in the analysis. The measurement is compared to earlier results at lower collision energies, and to theory predictions.

1 Introduction

The inclusive charged particle p_{T} spectrum is an important tool for studying high-p_{T} particle suppression in the dense QCD medium produced in high energy nucleus-nucleus (AA) collisions [1].

The modification of high-p_{T} particle production is typically quantified using the ratio of charged particle p_{T} spectra in nucleus-nucleus collisions to those in pp collisions scaled by the number of binary nucleon-nucleon collisions, N_{coll}. This quantity is known as the nuclear modification factor R_{AA} [1], and can be formulated as

$$R_{\mathrm{AA}}(p_{\mathrm{T}}) = \frac{d^2N^{\mathrm{AA}}/dp_{\mathrm{T}}d\eta}{T_{\mathrm{AA}}d^2\sigma^{\mathrm{NN}}/dp_{\mathrm{T}}d\eta}, \tag{1}$$

where $T_{\mathrm{AA}} = \langle N_{\mathrm{coll}}\rangle/\sigma^{\mathrm{NN}}_{\mathrm{inel}}$ is known as a nuclear overlap function and can be calculated from a Glauber model accounting for the nuclear collision geometry [2, 3].

The factor of 5 suppression observed using R_{AA} [4–7] at RHIC was an early indication of strong final-state medium effects on particle production. However, RHIC measurements were limited to a p_{T} range below 25 GeV. During the first two PbPb runs at the LHC, ALICE, ATLAS, and CMS measured the charged particle R_{AA} at 2.76 TeV collision energy per nucleon pairs up to a p_{T} of around 50 GeV (ALICE), and around 100 GeV (ATLAS, CMS), revealing a suppression by a factor of about 7 in the 5–10 GeV region [8–10]. At higher p_{T} this suppression was significantly reduced, approaching roughly a factor of 2 for particles with p_{T} in the range of 40–100 GeV. At the end of 2015, in the first heavy ion run of the Run-2 period of the LHC, PbPb collisions at $\sqrt{s_{\mathrm{NN}}} = 5.02$ TeV took place, allowing the experiments to study the suppression of charged particles at an unprecedented collision energy. Proton-proton reference data at the same collision energy were also provided, making direct comparisons between production cross sections measured in pp and PbPb collisions possible.

In this report, the measurement of the nuclear modification factor for primary charged particles produced in the $|\eta| < 1$ pseudorapidity range at $\sqrt{s_{\mathrm{NN}}} = 5.02$ TeV are presented. The measured nuclear modification factors are compared to earlier results at lower collision energies, as well as to model calculations.

2 The CMS detector, data selection, and MC samples

A detailed description of the CMS detector can be found in Ref. [11]. The CMS experiment uses a right-handed coordinate system, with the origin at the nominal interaction point and the z axis along the beam direction. The pseudorapidity η of a particle is defined as $\eta = -\ln[\tan(\theta/2)]$, where θ is the polar angle with respect to the proton beam direction. The silicon tracker, located in the 3.8 T magnetic field of the superconducting solenoid, is the detector subsystem used for the reconstruction of charged particles measured in this analysis. Consisting of 1440 silicon pixel and 15 148 silicon strip detector modules, with ≈10 million silicon strips and ≈ 60 million pixels, the silicon tracker measures charged particles within the pseudorapidity range $|\eta| < 2.5$. It provides a p_{T} resolution of about 1.5% for 100 GeV and 5% for 400 GeV charged particles. Also located inside the solenoid are an electromagnetic calorimeter (ECAL) and a hadron calorimeter (HCAL). The ECAL consists of lead tungstate crystals, arranged in a quasi-projective geometry, and distributed in a barrel region ($|\eta| < 1.48$) and in two endcaps that extend up to $|\eta| = 3.0$. The HCAL barrel and endcaps are sampling calorimeters composed of brass and scintillator plates, covering $|\eta| < 3.0$. Iron hadron forward calorimeters

(HF) with quartz fibers, read out by photomultipliers, extend the calorimeter coverage up to $|\eta| = 5.2$. An efficient muon system is deployed for the reconstruction and identification of muons up to $|\eta| = 2.4$. The detailed MC simulation of the CMS detector response is based on GEANT4 [12].

This analysis is performed using the 2015 pp and PbPb data taken at $\sqrt{s_{\mathrm{NN}}}$ = 5.02 TeV. The pp sample corresponds to an integrated luminosity of 25.8 pb^{-1}, while the PbPb sample corresponds to an integrated luminosity of 404 $\mu\mathrm{b}^{-1}$.

The CMS online event selection employs a hardware-based level-1 trigger (L1) and a software-based high level trigger (HLT). Minimum bias pp and PbPb collisions were selected using an HF-based L1 trigger requiring either single (pp) or coincidence (PbPb) signals above threshold. In order to extend the statistical reach of the measurement of R_{AA}, events selected by jet or high-p_{T} track triggers were also used.

In pp collisions, at L1 both the jet and the high-p_{T} track triggered events were selected by requiring the presence of L1-reconstructed jets above various calibrated transverse-momenta thresholds: 28, 40, and 48 GeV. While the first two triggers had to be prescaled because of the high instantaneous luminosity of the LHC, the highest threshold trigger always selected events unprescaled. At HLT, an online version of the offline jet and track reconstruction algorithms were run, optimized for fast execution. The high level jet triggers selected events with jets in the $|\eta| < 5.1$ region above a p_{T} of 40, 60, and 80 GeV, respectively, while the independent high-p_{T} track triggers looked for a track in the $|\eta| < 2.4$ region above transverse momenta of 12, 24, 34, 45, and 53 GeV, respectively. Only the highest-threshold triggers mentioned selected events unprescaled.

In PbPb collisions, the L1 jet triggers performed an event-by-event underlying-event subtraction, estimating the energy of the underlying event by averaging the deposited calorimeter transverse energies (E_{T}) in rings of ϕ as a function of η. The uncalibrated E_T thresholds of the PbPb L1 jet triggers were 28, 44, and 56 GeV. In the high level trigger for PbPb collisions, calorimeter jets were clustered with the anti-k_{T} algorithm after an event-by-event subtraction of the energy belonging to the heavy-ion underlying event was performed [13, 14]. Triggers with thresholds on the jet energy of 40, 60, 80, and 100 GeV were employed. Similarly to the case of pp collisions, only the highest threshold triggers mentioned above recorded data unprescaled. For the high-p_{T} track triggers deployed for PbPb collisions, a L1 requirement based on the E_{T} of highest-E_{T} calorimeter trigger region in the central $|\eta| < 1.044$ detector area was employed with thresholds of 16, and 24 GeV. At HLT, an online version of the PbPb track reconstruction algorithm (described in Section 3) was used to provide the trigger decision based on thresholds of p_{T} = 12, 18, 24, and 34 GeV. Both the jet and track triggers had variants only selecting PbPb collision events of specific centralities. This was made possible by an L1 algorithm, which estimated the collision centrality based on the sum of the E_{T} of the HF calorimeter regions. This analysis makes use of such triggers to enhance the event statistics in peripheral centrality bins. All the three described L1 algorithms were new in 2015, and were allowed by the upgrade of the CMS L1 system [15].

For the results described in this report, the jet-triggered data were used to provide access to the highest-p_{T} tracks. The track-triggered data were used as an alternative to the jet-triggered event sample in cross-check analyses.

Offline, events selected for analysis are expected to pass a set of selection criteria designed to reject events from background processes (beam-gas collisions, beam-scraping events). Events are required to have at least one reconstructed interaction vertex with at least two associated

tracks. In pp collisions, the events are also required to have at least 25% of the tracks meeting the so-called 'highPurity' requirement, which consists of separately trained MVA selectors for each tracking iteration (Section 3). In PbPb collisions, the shapes of the clusters in the pixel detector are required to be compatible with those expected in a PbPb collision. The event is also required to have at least three towers in both HF detectors with an energy deposit of more than 3 GeV per tower. The distortion of the shape of the p_T distribution due to the event selection requirements was corrected for in the pp data by evaluating the efficiency of the selection in "zero-bias" data. Zero bias data is selected solely based on whether there are filled bunches in coincidence in both beams crossing each other in the CMS interaction region. Thus, the zero bias dataset provides an unbiased sample to study the efficiency of the minimum-bias trigger and of the offline event selection. The distortion of the p_T spectrum in the measured p_T range due to the event selection was found to be smaller than 1% in pp data; although small this bias was corrected for. In PbPb data sample, the event selection is fully efficient in the centrality regions ($< 90\%$) used in this measurement.

To correct for inefficiencies associated with the track reconstruction algorithms, simulated samples are used. For pp collision data, these are PYTHIA8 [16] tune CUETP8M1 [17] minimum bias and dijet samples generated in different ranges of $\hat{p}_T$, the p_T of the hard collisions. For PbPb collision data, HYDJET 1.9 [18] minimum bias events and HYDJET-embedded PYTHIA dijet events are used. During the embedding procedure, a high-$\hat{p}_T$ PYTHIA event is merged with a minimum bias HYDJET event that matches the spatial position of the minimum-bias interaction.

The offline collision event centrality in PbPb events is determined from the total energy deposition in both HF calorimeters. The event centrality can be related to properties of the PbPb collisions such as the total number of binary nucleon-nucleon collisions (N_{coll}). The calculation of such properties is based on a Glauber model of the incoming nuclei [3] and studies of bin-to-bin smearing, caused by finite resolution effects and evaluated using fully simulated and reconstructed MC events [19]. The calculated N_{coll} and T_{AA} values corresponding to the centrality bins used in this report, along with their systematic uncertainties, are listed in Table 1. The uncertainties on the centrality variables are derived from propagating the uncertainties on the event selection efficiency and on the parameters of the Glauber model. The T_{AA} will be used in the calculation of the R_{AA} distributions.

3 Track reconstruction

In PbPb collisions, charged particles are reconstructed in a series of steps, which are similar to what was used in earlier work [20]. This procedure is based on the standard pp iterative tracking [21]. First, groups of three hits in the pixel tracker are used to reconstruct primary

Centrality	N_{coll}	T_{AA}
0–5%	1819 ± 126 (6.9%)	25.98 ± 0.431 (1.7%)
5–10%	1432 ± 98.6 (6.9%)	20.46 ± 0.351 (1.7%)
10–30%	805.4 ± 53.9 (6.7%)	11.51 ± 0.274 (2.4%)
30–50%	267.3 ± 19.7 (7.4%)	3.819 ± 0.188 (4.9%)
50–70%	65.41 ± 6.83 (10%)	0.9345 ± 0.0893 (9.6%)
70–90%	10.67 ± 1.73 (16%)	0.1525 ± 0.0245 (16%)
0–10%	1626 ± 112 (6.9%)	23.22 ± 0.392 (1.7%)
0–100%	392.5 ± 43.2 (11%)	5.607 ± 0.501 (8.9%)

Table 1: Summary of the N_{coll} and T_{AA} values and their uncertainties in $\sqrt{s_{NN}} = 5.02$ TeV PbPb collisions for the centrality bins used in this report.

vertex candidates, as well as seeds for track candidates. The seed trajectories are then propagated through the strip tracker to build fully reconstructed tracks. The procedure of propagating tracks through the detector is performed in five iterations, with each subsequent iteration removing hits unambiguously belonging to the tracks found in earlier iterations. The tracks found in the later iterations are merged with those found in earlier iterations after removing any duplicates, based on the fraction of shared hits and the χ^2 per number of degree of freedom, χ^2/ndf, of the track fit. For the analysis of pp data, the standard CMS pp tracking algorithm was used [21].

For both pp and PbPb data the standard 'highPurity' selection is used. To reduce the rate of misreconstructed tracks, particularly in high-occupancy central events, additional track selection cuts are applied. They are also used to enhance the fraction of tracks that are primary tracks originating from the primary interactions of the event. Only tracks with $|\eta| < 1$ are selected and are required to have a relative p_{T} error of less than 10% in PbPb collisions and 30% in pp collisions. Additionally, for tracks in PbPb collisions, requirements to have at least 11 hits along their trajectory in the pixel and strip tracking detectors, as well as having a χ^2/ndf divided by the total number of tracker layers hit along the track trajectory less than 0.15, are imposed. To decrease the likelihood of counting tracks from secondary decay products, a selection requirement of 3σ is applied on the distance of closest approach to at least one primary vertex in the event for both collision systems.

Finally, a cut based on a track's relationship to calorimeter energy deposits in the event is applied in order to curtail the contribution of very high p_{T} misreconstructed tracks. Tracks above a p_{T} of 20 GeV are required to have an associated energy deposit of at least half their momentum in the CMS calorimeters. The requirement of 50% was determined by comparing the distributions of the associated deposits for real and fake tracks in simulated events to tracks reconstructed in real data. The efficiency of the calorimeter-matching requirement is 95% in pp and 98% in PbPb data for tracks selected for analysis by the other track-selection criteria.

To calculate the corrections in PbPb data for tracking efficiency and detector acceptance, a large sample of simulated PYTHIA events are used after being embedded and reconstructed in PbPb minimum-bias events generated with HYDJET. The corrections are applied on a track-by-track basis, and take into account properties of the track and event: the track p_{T}, position in the detector acceptance, event centrality, and radial distance of the track from jets. The dependence of the efficiency and misreconstruction fraction is assumed to be uncorrelated in each of these variables for tracks having similar properties. The efficiency of the PbPb track reconstruction algorithm and track selection for minimum-bias events is approximately 40% at 0.7 GeV, then it increases rapidly to around 65% at 1 GeV, where it reaches a plateau. The efficiency starts to decrease from p_{T} values of around 100 GeV until it reaches about 50% at 400 GeV. The efficiency is also centrality dependent; the average efficiency is approximately 60% for central events, while peripheral events have average efficiencies of 75%. In general, the misreconstruction rate is very small due to the strict selection criteria applied to the tracks. The rate does increase at low track p_{T} and also slightly at very high p_{T}, to around 3%. The misreconstruction rate under 1 GeV increases to 10% in the most central events.

For pp collisions, the tracking corrections are derived from a sample of simulated PYTHIA events. The efficiency is between 80 and 90% for most of the p_{T} range studied here, except at p_{T} greater than 150 GeV, where it decreases to 70%. The misreconstruction rate in pp is found to be less than 3%.

The p_{T} resolution of selected tracks is excellent, remaining below 2% up to about 100 GeV. For higher p_{T} it starts to increase reaching about 6% at transverse momentum of about 400 GeV.

The resulting distortion of the reconstructed p_T distribution introduced by the track resolution was found to be less than 1%. This distortion is not corrected for, but is accounted for in the systematic uncertainty.

Particles of different species have different track reconstruction efficiencies for a given particle p_T. As different Monte Carlo event generators model the relative fractions of the particle species differently, the computed tracking efficiencies for inclusive primary charged particles depend on which MC generator is used to evaluate the correction. Notably, the reconstruction efficiency for primary charged strange baryons is very low, as they decay before leaving a sufficient number of tracker hits for direct reconstruction. However, the fraction of these particles varies significantly between different models. In this measurement, the species-dependent track reconstruction efficiencies were convoluted with the corresponding particle fractions according to PYTHIA8 CUETP8M1 and according to EPOS [22] tune LHC [23], and the two sets of correction factors averaged.

4 Combination of particle spectra

To obtain the inclusive charged particle spectra up to a few hundred GeV, data recorded by the minimum-bias and by the jet triggers are combined. The procedure to combine the spectra was already developed and applied in earlier CMS publications [10, 24].

The event-weight factors corresponding to the various triggers are computed by counting the number of events that contain leading jets (defined as the jets with the highest p_T in the event) in the range of $|\eta| < 2$ with p_T values in regions not affected by trigger thresholds, i.e., where the trigger efficiency of the higher-threshold trigger is constant relative to that of the lower-threshold trigger. The ratio of the number of such events in the two triggered sets of data are used as weight factors. For example, the region above which the jet trigger with a p_T threshold of 40 GeV has constant efficiency is determined by comparing the p_T distribution of the leading jets to that of the minimum-bias data. Similarly, the constant efficiency region of the 60 GeV jet trigger is determined by comparison to the 40 GeV jet trigger, and so on.

To determine the inclusive particle spectrum, events are first uniquely classified into leading-jet p_T classes. The spectra are constructed by taking events from the minimum-bias, 40 GeV jet, 60 GeV jet triggers, respectively, for each bin. The particle spectra are evaluated in each bin separately, then combined using the normalization factors described in the previous paragraph. The procedure outlined above was verified in a data driven way by constructing a charged-particle spectrum from an alternative combination of event samples triggered by high-p_T tracks. The final spectra are found to be consistent with each other. For the overall normalization of the combined spectra, in PbPb collisions the number of minimum-bias events in the particular centrality bins are used, while in pp collisions the normalization is determined by the integrated luminosity.

The ratio of the normalized distribution of the leading-jet p_T from minimum-bias and from various jet-triggered data in PbPb collisions in the 0–30% centrality bin can be seen in the left panel of Fig. 1. The constant-efficiency regions are selected to be above p_T of 60, 80, 100, and 120 GeV for the Jet40, Jet60, Jet80, and Jet100 triggers, respectively.

The contribution from each of the datasets selected by the different jet trigger thresholds to the combined, but otherwise uncorrected, track spectrum can be seen in the right panel of Fig. 1. The combined spectrum includes contributions from each jet trigger threshold dataset at each charged particle p_T bin, although the relative contributions of the different datasets naturally

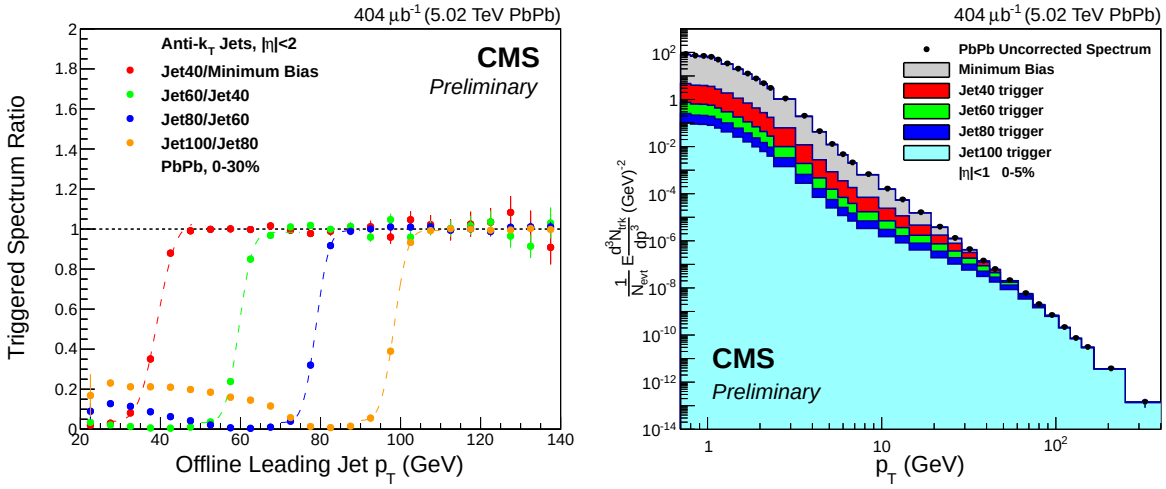

Figure 1: *Left:* ratio of the leading-jet p_{T} distributions in PbPb collisions in the 0–30% centrality bin from various triggers, after the data have been normalized to one another. For better visibility, lines were added to guide the eye. *Right:* contributions from the various jet triggers (colored histograms) to the combined, but otherwise uncorrected, track spectrum (black markers) in the 0–5% centrality bin.

varies strongly as a function of p_{T}.

5 Systematic studies and uncertainties

The systematic uncertainties influencing the measurement of the nuclear modification factor are presented in Table 2. The ranges quoted cover both the p_{T} and the centrality dependence of the uncertainties.

- **Event-selection correction** The bias resulting from the event selection conditions on the shape of the R_{AA} distribution was corrected by a data-driven procedure (Section 2). To estimate the corresponding systematic uncertainty, the event selection correction was also evaluated using simulated events. The charged particle R_{AA} distribution, reconstructed with the MC-based alternative event selection correction, was found to differ by less than 1% from the main result.
- **Momentum resolution** The distortion effect of the resolution of the track reconstruction on the measured charged particle p_{T} distribution was evaluated using simulated events. The resulting distortion was found to be less than 1.5%; this value is conservatively assigned as the associated systematic uncertainty on R_{AA}.
- **Particle species composition** As described in Section 3, the tracking corrections used in the analysis correspond to a particle species composition that lies halfway between that in PYTHIA8 CUETP8M1 and EPOS. We assign the difference in tracking efficiency from the corrections given by the pure PYTHIA8 CUETP8M1 or the pure EPOS particle composition as a systematic uncertainty. The systematic uncertainty has a strong p_{T} dependence. Below a p_{T} of around 1.5 GeV and above of about 10 GeV, the uncertainty is 1.5%. Between these p_{T} values, the uncertainty increases rapidly with p_{T}, reaching a value of about 15.5% at 3 GeV, followed by a steady decrease to 1.5% at and above 10 GeV. The uncertainties were evaluated in bins of centrality, resulting in higher uncertainties for more central events.

Sources	Uncertainty [%]
Event-selection correction	<1
Momentum resolution	1.5
Particle species composition	1.5–15.5
Fraction of misreconstructed tracks	3
Tracking correction non-closure	5
Tracking efficiency	6.5
Track selection	4
Pileup	3
Trigger combination	0–2.5
Luminosity	12
Glauber-model uncertainty	1.7–16
R_{AA} uncertainty	10–17

Table 2: Systematic uncertainties associated with the charged particle R_{AA} measurement. The ranges quoted cover both the p_{T} and the centrality dependence of the uncertainties. The uncertainty of R_{AA} quoted in the table does not include the luminosity and the T_{AA} uncertainties.

- **Fraction of misreconstructed tracks** The fraction of misreconstructed tracks is computed from simulated events. To account for possible differences in the misreconstruction fraction between simulated and real events, the total amount of the correction is assigned as systematic uncertainty.
- **Tracking correction non-closure** The accuracy of the tracking correction procedure was tested in simulated events by comparing the fully corrected track spectrum to the spectrum of simulated particles. In such comparisons, differences smaller than 5% were observed. This 5% 'non-closure' of the tracking corrections was conservatively assigned as systematic uncertainty for the measured R_{AA} distributions. The main source of the non-closure is the only approximate validity of the assumption that the track p_{T}, the track $\eta - \phi$, the event centrality, and the radial distance of tracks from jets variables factorize in the bins of track p_{T} and event centrality used for the calculation of tracking correction factors.
- **Tracking efficiency** The difference in the track reconstruction efficiency in pp data and pp simulation was studied by comparing the relative fraction of reconstructed D^* mesons in the three-prong and five-prong decay channels in simulated and real events [25]. Based on the difference seen between the two in the relative branching fractions, and on direct comparison made between track quality variables in data and simulation, a conservative 6.5% systematic uncertainty was assigned as coming from the modelling of the tracking efficiency.
- **Track selection** The reconstruction of charged particle spectra was repeated using alternative track selection criteria, as well as using track triggers instead of jet triggers. Based on the differences observed in the fully corrected R_{AA}, a conservative 4% systematic uncertainty was assigned.
- **Pileup** For pp collisions, the average pileup (the mean of the Poisson distribution of the number of collisions per bunch crossings) was approximately 1.4. In the analysis, tracks compatible with any of the primary vertices are selected. To assess the possible effect of pileup on the particle spectrum, the spectrum was recomputed using only single-vertex collision events. Based on the differences observed in the shape of the spectrum, a systematic uncertainty of 3% was evaluated.

- **Luminosity** The uncertainty on the preliminary integrated luminosity for pp collisions is 12%.
- **Trigger combination** The method of combining the different triggers used in this analysis relies on the calculation of overlaps in the leading jet spectra between the different triggers. The calculated trigger weights are subject to fluctuations due to only having finite statistics. To assess the corresponding uncertainty on R_{AA}, the uncertainties on the trigger weights associated to each trigger path were weighted according to the fraction of the particle spectrum that the trigger contributes in a given p_{T} bin. The overall uncertainty was found to range from negligible to 2.5%. The uncertainty is highest for peripheral events and increases with p_{T}.
- **Glauber-model uncertainty** The systematic uncertainty on the Glauber-model normalization factors (T_{AA}) ranges from 1.7% (in the 0–5% bin) to 16% (in the 70–90% centrality bin). The uncertainties on the T_{AA} values are derived from propagating the uncertainties on the event selection efficiency and on the parameters of the Glauber model.

6 Results

The measured nuclear modification factors for primary charged particles in PbPb collisions at $\sqrt{s_{\mathrm{NN}}} = 5$ TeV in the 0–5%, 5–10%, 10–30%, 30–50%, 50–70%, and 70–90% centrality bins are shown in Fig. 2. The result for the inclusive 0–100% centrality range is shown in Appendix A. The error bars represent the statistical uncertainties, the blue and gray error boxes around 1 show the Glauber-model-related T_{AA} and the pp luminosity uncertainties, respectively, while the yellow band represents the other systematic uncertainties discussed in Section 5. The R_{AA} distributions show larger suppression for more head-on collisions, reaching a suppression of a factor of about 7.5 in the 0–5% centrality bin for transverse momenta of around 6–9 GeV. At larger p_{T}, R_{AA} appears to exhibit a continuous rise up to the highest p_{T} values measured. The uncertainties show a characteristic broadening in the 2–10 GeV p_{T} region, where the uncertainty due to the particle composition is the largest.

In Fig. 3, the measured R_{AA} distributions at $\sqrt{s_{\mathrm{NN}}} = 5.02$ TeV are compared to the CMS measurements at $\sqrt{s_{\mathrm{NN}}} = 2.76$ TeV [10]. Additionally, for the 0–5% bin, results from ALICE [8] and ATLAS [9] are also shown. The error bars represent the statistical uncertainties, while the boxes indicate the systematic uncertainties on the 5 TeV CMS measurement. At low p_{T}, the 2.76 and 5.02 TeV measurements are in good agreement in all centrality bins. Above about 10 GeV, the R_{AA} values at 5.02 TeV tend to be slightly lower than at 2.76 TeV, especially for central collisions. Given that the charged particle spectrum flattens out at high p_{T} with increasing collision energy, similar R_{AA} values measured at 2.76 and 5.02 TeV point to a larger average energy loss in the higher-energy collisions at a fixed p_{T} [1].

The measured R_{AA} distributions in the 0–10% and 30–50% centrality bins are compared to the predictions from the models described in Refs. [26] and [27] in Fig. 4. The $\mathrm{SCET_G}$ model [26] is based on the generalization of the DGLAP evolution equations to include final-state medium-induced parton showers combined with initial-state effects. This model gives a good description of the measured data over the 5–200 GeV transverse momentum range. The CUJET3.0 model [27] is constructed by generalizing the perturbative-QCD based CUJET2.0 model to include two complementary non-perturbative features of the QCD confinement cross-over phase transition: i) suppression of quark and gluon degrees of freedom, and ii) the emergence of chromo-magnetic monopole degrees of freedom. The model predicts a charged particle suppression larger than seen in data.

The evolution of the nuclear modification factor with center-of-mass energy, from the SPS [28, 29] to RHIC [30, 31] and then to the LHC [8–10], is presented in Fig. 5. The data from this analysis is shown by the black dots. The error bars show the statistical uncertainties, while the yellow band surrounding the new 5 TeV CMS points represent the systematic uncertainties, including that of the luminosity (in the previous figures the luminosity uncertainty was shown along with the Glauber-model uncertainty as a separate error box around unity). Errors less than 5% due to Glauber-model uncertainty are not included in the figure. The prediction of the models of Refs. [26, 27] are also shown.

The presented charged particle R_{AA} distributions help to illuminate the mechanisms for jet quenching and the properties of the medium produced in heavy-ion collisions. Together with measurements on high-p_{T} charged particle azimuthal anisotropies, inclusive jet spectra, fragmentation functions, γ-jet and Z-jet correlations, it constrains the possible phase space of parameters for models aiming to describe the main features of heavy-ion collisions.

References

[1] D. d'Enterria, "Jet quenching", *Landolt-Bornstein* **23** (2010) 471, doi:10.1007/978-3-642-01539-7_16, arXiv:0902.2011.

[2] M. L. Miller, K. Reygers, S. J. Sanders, and P. Steinberg, "Glauber modeling in high energy nuclear collisions", *Ann. Rev. Nucl. Part. Sci.* **57** (2007) 205, doi:10.1146/annurev.nucl.57.090506.123020, arXiv:nucl-ex/0701025.

[3] B. Alver et al., "Importance of correlations and fluctuations on the initial source eccentricity in high-energy nucleus-nucleus collisions", *Phys. Rev. C* **77** (2008) 014906, doi:10.1103/PhysRevC.77.014906, arXiv:0711.3724.

[4] BRAHMS Collaboration, "Quark Gluon Plasma an Color Glass Condensate at RHIC? The perspective from the BRAHMS experiment", *Nucl. Phys. A* **757** (2005) 1, doi:10.1016/j.nuclphysa.2005.02.130, arXiv:nucl-ex/0410020.

[5] PHENIX Collaboration, "Formation of dense partonic matter in relativistic nucleus nucleus collisions at RHIC: Experimental evaluation by the PHENIX collaboration", *Nucl. Phys. A* **757** (2005) 184, doi:10.1016/j.nuclphysa.2005.03.086, arXiv:nucl-ex/0410003.

[6] STAR Collaboration, "Experimental and theoretical challenges in the search for the quark gluon plasma: The STAR collaboration's critical assessment of the evidence from RHIC collisions", *Nucl. Phys. A* **757** (2005) 102, doi:10.1016/j.nuclphysa.2005.03.085, arXiv:nucl-ex/0501009.

[7] B. B. Back et al., "The PHOBOS perspective on discoveries at RHIC", *Nucl. Phys. A* **757** (2005) 28, doi:10.1016/j.nuclphysa.2005.03.084, arXiv:nucl-ex/0410022.

[8] ALICE Collaboration, "Centrality Dependence of Charged Particle Production at Large Transverse Momentum in Pb–Pb Collisions at $\sqrt{s_{\mathrm{NN}}} = 2.76$ TeV", *Phys. Lett. B* **720** (2013) 52, doi:10.1016/j.physletb.2013.01.051, arXiv:1208.2711.

[9] ATLAS Collaboration, "Measurement of charged-particle spectra in Pb+Pb collisions at $\sqrt{s_{\mathrm{NN}}} = 2.76$ TeV with the ATLAS detector at the LHC", *JHEP* **09** (2015) 050, doi:10.1007/JHEP09(2015)050, arXiv:1504.04337.

[10] CMS Collaboration, "Study of high-pT charged particle suppression in PbPb compared to pp collisions at $\sqrt{s_{NN}} = 2.76$ TeV", *Eur. Phys. J. C* **72** (2012) 1945, doi:10.1140/epjc/s10052-012-1945-x, arXiv:1202.2554.

[11] CMS Collaboration, "The CMS experiment at the CERN LHC", *JINST* **3** (2008) S08004, doi:10.1088/1748-0221/3/08/S08004.

[12] GEANT4 Collaboration, "GEANT4: A Simulation toolkit", *Nucl. Instrum. Meth. A* **506** (2003) 250, doi:10.1016/S0168-9002(03)01368-8.

[13] M. Cacciari, G. P. Salam, and G. Soyez, "The anti-k_t jet clustering algorithm", *JHEP* **04** (2008) 063, doi:10.1088/1126-6708/2008/04/063, arXiv:0802.1189.

[14] O. Kodolova, I. Vardanian, A. Nikitenko, and A. Oulianov, "The performance of the jet identification and reconstruction in heavy ions collisions with CMS detector", *Eur. Phys. J. C* **50** (2007) 117, doi:10.1140/epjc/s10052-007-0223-9.

[15] CMS Collaboration, "Run 2 Upgrades to the CMS Level-1 Calorimeter Trigger", *JINST* **11** (2016) C01051, doi:10.1088/1748-0221/11/01/C01051, arXiv:1511.05855.

[16] T. Sjostrand, S. Mrenna, and P. Z. Skands, "A Brief Introduction to PYTHIA 8.1", *Comput. Phys. Commun.* **178** (2008) 852, doi:10.1016/j.cpc.2008.01.036, arXiv:0710.3820.

[17] CMS Collaboration, "Event generator tunes obtained from underlying event and multiparton scattering measurements", *Eur. Phys. J. C* **76** (2016) 155, doi:10.1140/epjc/s10052-016-3988-x, arXiv:1512.00815.

[18] I. P. Lokhtin and A. M. Snigirev, "A Model of jet quenching in ultrarelativistic heavy ion collisions and high-p(T) hadron spectra at RHIC", *Eur. Phys. J. C* **45** (2006) 211, doi:10.1140/epjc/s2005-02426-3, arXiv:hep-ph/0506189.

[19] CMS Collaboration, "Observation and studies of jet quenching in PbPb collisions at nucleon-nucleon center-of-mass energy = 2.76 TeV", *Phys. Rev. C* **84** (2011) 024906, doi:10.1103/PhysRevC.84.024906, arXiv:1102.1957.

[20] CMS Collaboration, "Measurement of transverse momentum relative to dijet systems in PbPb and pp collisions at $\sqrt{s_{\mathrm{NN}}} = 2.76$ TeV", *JHEP* **01** (2016) 006, doi:10.1007/JHEP01(2016)006, arXiv:1509.09029.

[21] CMS Collaboration, "Tracking and Vertexing Results from First Collisions", *CMS Physics Analysis Summary* **CMS-PAS-TRK-10-001** (2010).

[22] K. Werner, F.-M. Liu, and T. Pierog, "Parton ladder splitting and the rapidity dependence of transverse momentum spectra in deuteron-gold collisions at RHIC", *Phys. Rev. C* **74** (2006) 044902, doi:10.1103/PhysRevC.74.044902, arXiv:hep-ph/0506232.

[23] T. Pierog et al., "EPOS LHC: Test of collective hadronization with data measured at the CERN Large Hadron Collider", *Phys. Rev. C* **92** (2015) 034906, doi:10.1103/PhysRevC.92.034906, arXiv:1306.0121.

[24] CMS Collaboration, "Nuclear Effects on the Transverse Momentum Spectra of Charged Particles in pPb Collisions at $\sqrt{s_{\mathrm{NN}}} = 5.02$ TeV", *Eur. Phys. J. C* **75** (2015) 237, doi:10.1140/epjc/s10052-015-3435-4, arXiv:1502.05387.

[25] CMS Collaboration, "Measurement of Tracking Efficiency", *CMS Physics Analysis Summary* **CMS-PAS-TRK-10-002** (2010).

[26] Y.-T. Chien et al., "Jet Quenching from QCD Evolution", *Phys. Rev. D* **93** (2016) 074030, doi:10.1103/PhysRevD.93.074030, arXiv:1509.02936.

[27] J. Xu, J. Liao, and M. Gyulassy, "Bridging Soft-Hard Transport Properties of Quark-Gluon Plasmas with CUJET3.0", *JHEP* **02** (2016) 169, doi:10.1007/JHEP02(2016)169, arXiv:1508.00552.

[28] WA98 Collaboration, "Transverse mass distributions of neutral pions from Pb-208 induced reactions at 158-A-GeV", *Eur. Phys. J. C* **23** (2002) 225, doi:10.1007/s100520100886, arXiv:nucl-ex/0108006.

[29] D. G. d'Enterria, "Indications of suppressed high p_{T} hadron production in nucleus - nucleus collisions at CERN-SPS", *Phys. Lett. B* **596** (2004) 32, doi:10.1016/j.physletb.2004.06.071, arXiv:nucl-ex/0403055.

[30] PHENIX Collaboration, "Neutral pion production with respect to centrality and reaction plane in Au+Au collisions at $\sqrt{s_{NN}}$ = 200 GeV", *Phys. Rev. C* **87** (2013) 034911, doi:10.1103/PhysRevC.87.034911, arXiv:1208.2254.

[31] STAR Collaboration, "Transverse momentum and collision energy dependence of high p_{T} hadron suppression in Au+Au collisions at ultrarelativistic energies", *Phys. Rev. Lett.* **91** (2003) 172302, doi:10.1103/PhysRevLett.91.172302, arXiv:nucl-ex/0305015.

[32] NA49 Collaboration, "High transverse momentum hadron spectra at $\sqrt{s_{NN}} = 17.3$ GeV, in Pb+Pb and p+p collisions", *Phys. Rev. C* **77** (2008) 034906, doi:10.1103/PhysRevC.77.034906, arXiv:0711.0547.

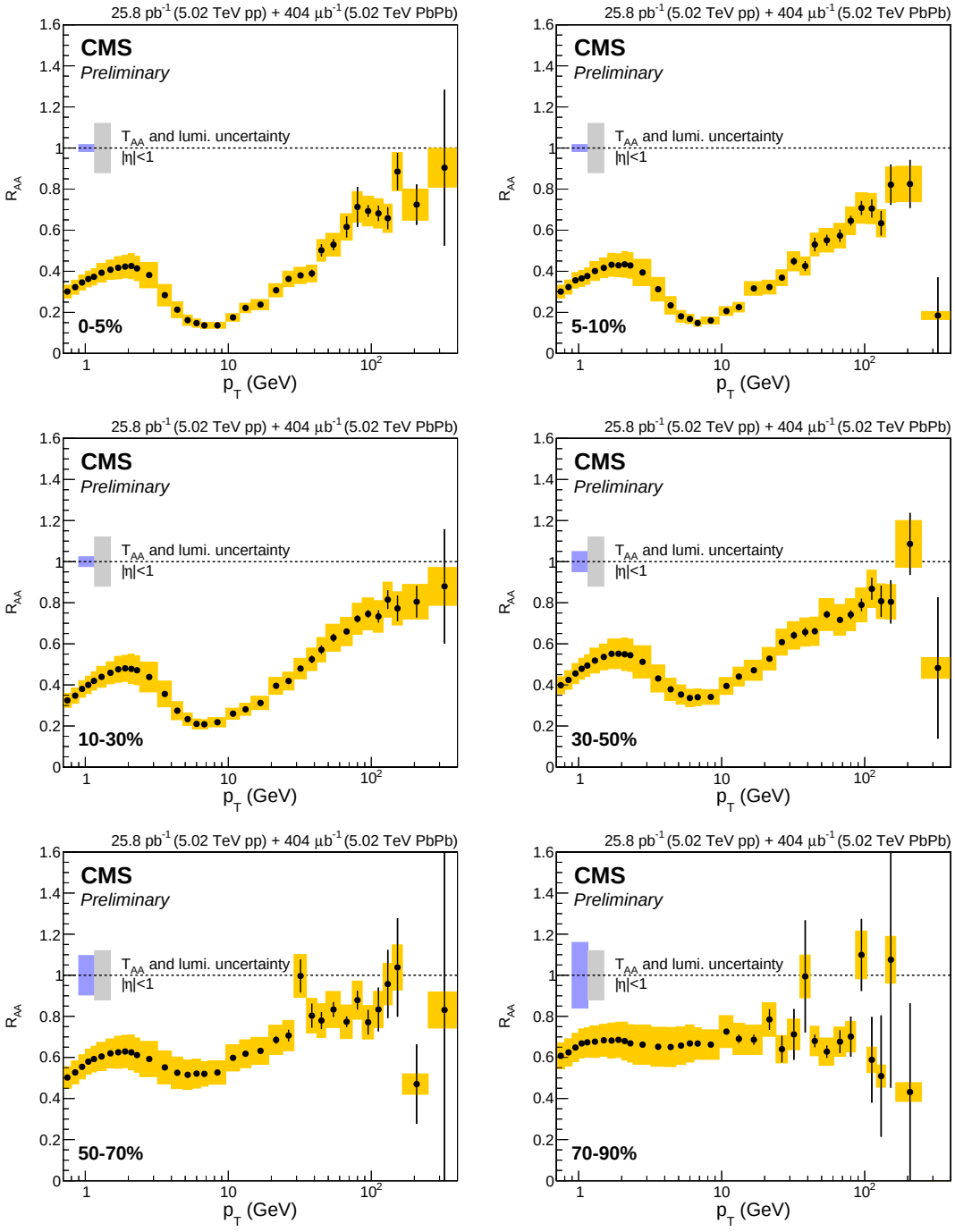

Figure 2: Charged particle R_{AA} measured in six different centrality ranges in PbPb collisions at $\sqrt{s_{\mathrm{NN}}} = 5.02$ TeV collision energy. The error bars represent the statistical uncertainties, the blue and gray error boxes around 1 show the Glauber-model-related T_{AA} and the pp luminosity uncertainties, respectively, while the yellow band represents all other systematic uncertainties.

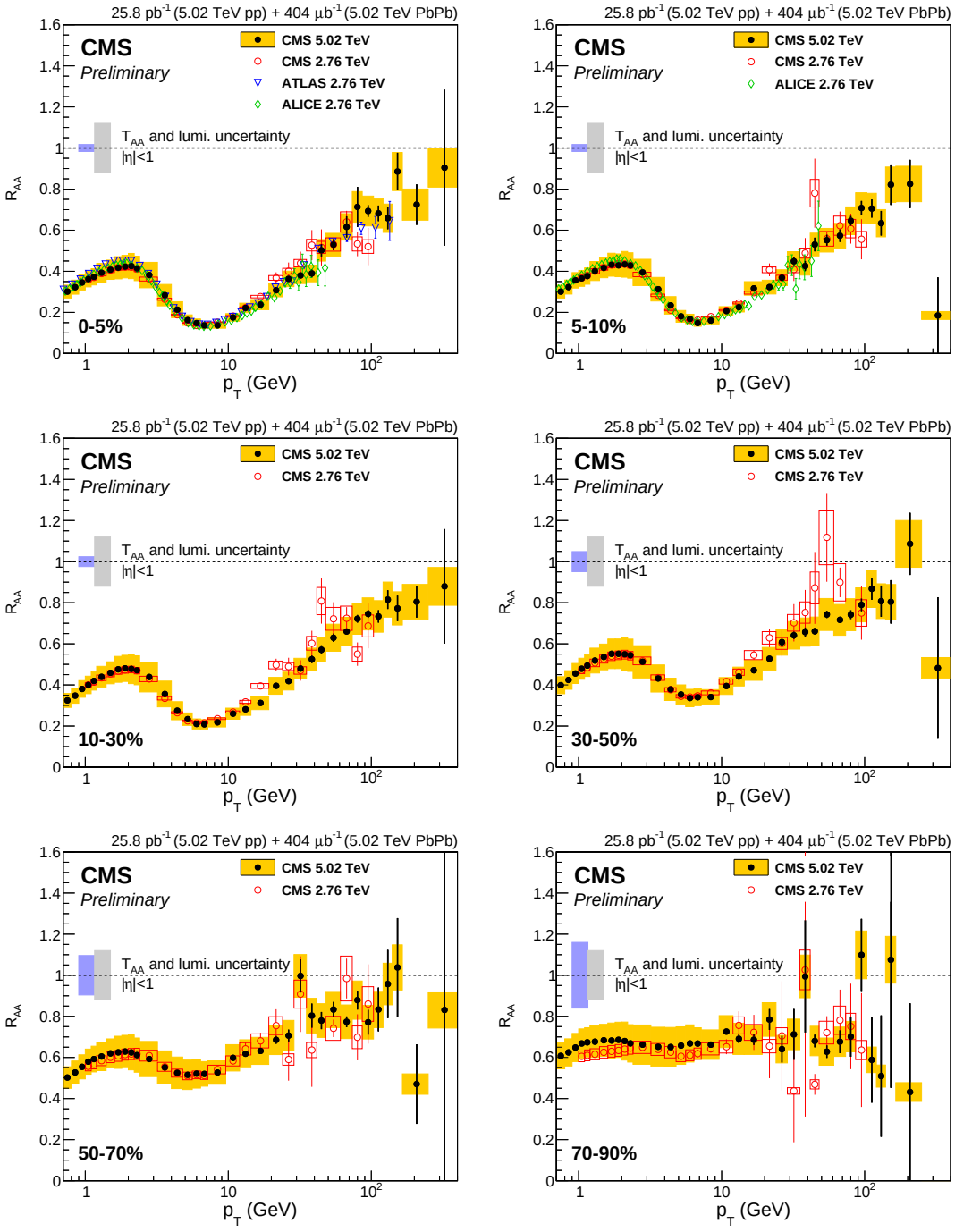

Figure 3: Charged particle R_{AA} measured in six different centrality ranges at $\sqrt{s_{\mathrm{NN}}} = 5.02$ TeV compared to CMS [10] (all centrality bins), ALICE [8] (in the 0–5% and 5–10% centrality bins) and ATLAS [9] (in the 0–5% centrality bin) results at a center-of-mass energy per nucleon pair of 2.76 TeV.

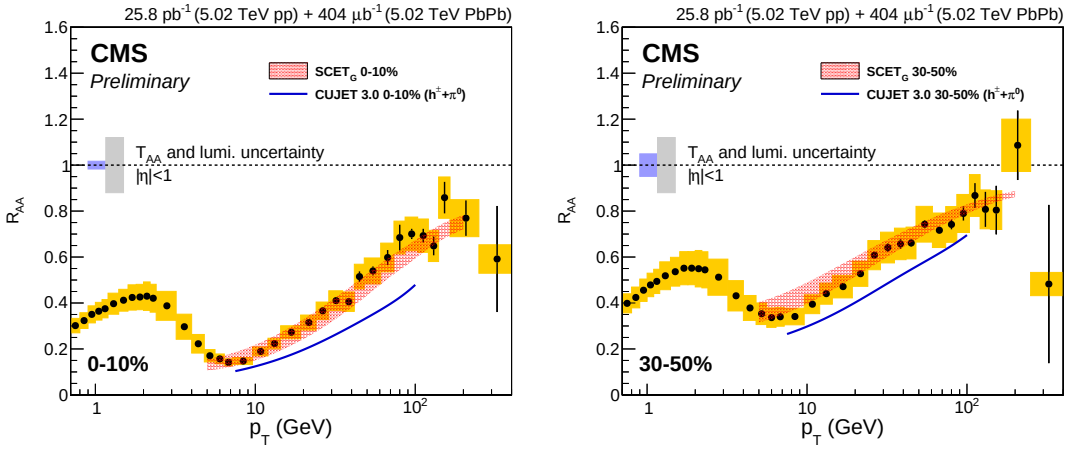

Figure 4: Charged particle R_{AA} measured in the 0–10% (left) and 30–50% (right) centrality ranges at $\sqrt{s_{\mathrm{NN}}} = 5.02$ TeV compared to predictions of models from Refs. [26] and [27].

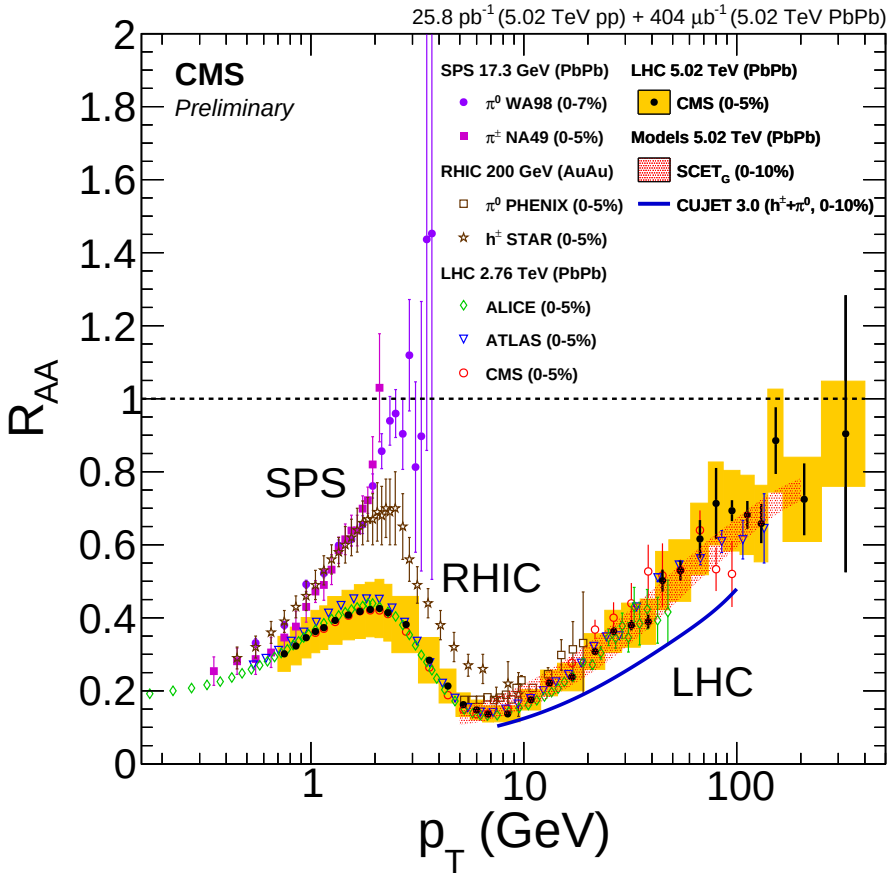

Figure 5: Measurements of the nuclear modification factors in central heavy-ion collisions at four different center-of-mass energies, for neutral pions (π^0) (SPS, RHIC), charged hadrons ($h^{\pm}$) (SPS, RHIC), and charged particles (LHC), from Refs. [8–10, 28–32], compared to predictions of two models from Refs. [26, 27]. The error bars represent the statistical uncertainties. The yellow band around the 5 TeV CMS data shows the systematic uncertainties of the measurement, including that of the luminosity. The T_{AA} uncertainties, of the order of $\pm 5\%$, are not shown.

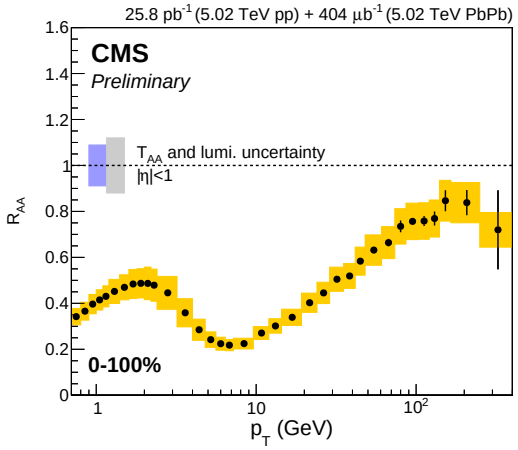

Figure 6: Charged particle R_{AA} measured in the inclusive 0–100% centrality range in PbPb collisions at $\sqrt{s_{\mathrm{NN}}} = 5.02$ TeV collision energy. The error bars represent the statistical uncertainties, the blue and gray error boxes around unity show the Glauber-model-related T_{AA} and the pp luminosity uncertainties, respectively, while the yellow band represents all other systematic uncertainties.

A Supplementary material

The measured charged particle R_{AA} for the inclusive 0–100% centrality range is presented in Fig. 6. For the measurement, an event selection efficiency of $99 \pm 2\%$ is used (selection efficiencies higher than 100% are possible, reflecting the presence of ultra-peripheral collisions in our selected event sample). The 2% uncertainty is included in the yellow systematic uncertainty band.